

Universal Scaling Laws for Correlation Spreading in Quantum Systems with Short- and Long-Range Interactions

Lorenzo Cevolani,¹ Julien Despres,^{2,3} Giuseppe Carleo,⁴ Luca Tagliacozzo,⁵ and Laurent Sanchez-Palencia²

¹*Institut für Theoretische Physik, Georg-August-Universität Göttingen, 37077 Göttingen, Germany*

²*Centre de Physique Théorique, Ecole Polytechnique, CNRS, Univ Paris-Saclay, F-91128 Palaiseau, France*

³*Laboratoire Charles Fabry, Institut d'Optique, CNRS, Univ Paris-Saclay, 2 avenue Augustin Fresnel, F-91127 Palaiseau cedex, France*

⁴*Institute for Theoretical Physics, ETH Zurich, Wolfgang-Pauli-Str. 27, 8093 Zurich, Switzerland*

⁵*Department of Physics and SUPA, University of Strathclyde, Glasgow G4 0NG, United Kingdom*

(Dated: August 31, 2022)

We study the spreading of information in a wide class of quantum systems, with variable-range interactions. We show that, after a quench, it generally features a double structure, whose scaling laws are related to a set of universal microscopic exponents that we determine. When the system supports excitations with a finite maximum velocity, the spreading shows a twofold ballistic behavior. While the correlation edge spreads with a velocity equal to twice the maximum group velocity, the dominant correlation maxima propagate with a different velocity that we derive. When the maximum group velocity diverges, as realizable with long-range interactions, the correlation edge features a slower-than-ballistic motion. The motion of the maxima is, instead, either faster-than-ballistic, for gapless systems, or ballistic, for gapped systems. The phenomenology that we unveil here provides a unified framework, which encompasses existing experimental observations with ultracold atoms and ions. It also paves the way to simple extensions of those experiments to observe the structures we describe in their full generality.

Introduction. – The ability of a quantum system to establish long-distance correlations and entanglement, as well as mutual equilibrium between distant parts, is determined by the speed at which information can propagate throughout the system. For lattice models with short-range interactions, Lieb and Robinson have demonstrated the existence of a maximum propagation speed limit, even for non-relativistic theories. This bound sets a linear causality cone beyond which correlations decay exponentially [1]. In a large class of many-body systems the information is carried by quasi-particles and the cone velocity may be related to their maximum velocity [2, 3], whenever it exists. Ballistic propagation of quantum correlations has received experimental [4, 5] and numerical [6–8] assessment, with, however, a cone velocity that may significantly differ from that expected.

For long-range interactions, a different form of causality arise due to direct coupling between local observables at arbitrary long distances. Long-range interactions appear in a variety of contexts, including van der Waals interactions Rydberg atom gases [9–12], effective photon-photon interactions in nonlinear media [13], dipole-dipole interactions between polar molecules [14–16] and magnetic atoms [17–21], photon-mediated interactions in superconductors [22] and artificial ion crystal [23–27], and solid-state defects [28–30]. They can be modelled by couplings decaying algebraically, $1/R^\alpha$, with the distance R . For such systems, known extensions of the Lieb-Robinson (LR) bound in D dimensions include a logarithmic bound, $t^* \sim \log(R)$, for $\alpha > D$ [31] and an algebraic bound, $t^* \sim R^\beta$ with $\beta < 1$, for $\alpha > 2D$ [32]. In both cases, they are super-ballistic. No bound is known

for $\alpha < D$, which in principle allows for instantaneous propagation.

Information spreading in systems with long-range interactions has been intensively studied, in a variety of models, both experimentally and numerically. On the one hand, there is a consensual agreement that long-range LR bounds are usually too loose to predict the actual dynamics. On the other hand, they appear to be strongly model dependent, and seemingly contradictory. For instance, for the long-range XY (LRXY) model in one dimension, super-ballistic propagation has been reported in ion chains [33] and numerical simulations within truncated Wigner approximation [34], even for $\alpha < 1$. Conversely, for the long-range transverse Ising (LRTI) model, experiments reported ballistic propagation irrespective to the value of α [35]. Moreover, time-dependent density matrix renormalization group (t-DMRG) and variational Monte-Carlo (t-VMC) numerical simulations indicate instantaneous, sub-ballistic, and ballistic spreading laws for increasing values of the exponent α [36–41].

Here, we provide a universal picture of correlation spreading in generic quantum lattice models with variable-range interactions. We show that, generally, the space-time correlation map features a twofold causality structure. While the outer structure determines the LR edge, the inner structure determines the propagation of local maxima. For short-range interactions, they are both determined by the many-body dispersion relation and can be associated, respectively, to the group and phase velocities. For intermediate long-range interactions, the inner structure is also completely determined by the dispersion relation and strongly depends on its

nature. It is super-ballistic for gapless systems and ballistic for gapped systems. In turn, the outer structure depends on the dispersion relation, but not on the gap, and depends on the observable. It is always sub-ballistic, except for observables with a strong infrared divergence. Our results shed new light on correlation spreading in quantum systems and provides a unified picture to interpret previous results present in the literature.

Time evolution of local observables. – Consider a quantum system defined on an hypercubic lattice of dimension D and governed by the Hamiltonian

$$\hat{H} = \sum_{\mathbf{R}} h(\mathbf{R}) \hat{K}_1(\mathbf{R}) + \sum_{\mathbf{R}, \mathbf{R}'} J(\mathbf{R}, \mathbf{R}') \hat{K}_2(\mathbf{R}, \mathbf{R}'), \quad (1)$$

where $\mathbf{R}, \mathbf{R}' \in \mathbb{Z}^D$ span the lattice sites. The first term accounts for local interaction with an external field $h(\mathbf{R})$ via the one-site operators $\hat{K}_1(\mathbf{R})$. The second term describes off-diagonal coupling of amplitude $J(\mathbf{R}, \mathbf{R}')$ via the two-site operators $\hat{K}_2(\mathbf{R}, \mathbf{R}')$. The generic Hamiltonian (1) applies to a variety of systems. In the following, we consider both quantum particle or spin models. The Bose-Hubbard model is constructed using the particle operators $K_1(\mathbf{R}) \equiv \hat{n}_{\mathbf{R}}(\hat{n}_{\mathbf{R}} - 1)$ and $K_2(\mathbf{R}, \mathbf{R}') \equiv -\hat{a}_{\mathbf{R}}^\dagger \hat{a}_{\mathbf{R}'} - \hat{a}_{\mathbf{R}'}^\dagger \hat{a}_{\mathbf{R}}$, where $\hat{a}_{\mathbf{R}}$ and $\hat{n}_{\mathbf{R}} = \hat{a}_{\mathbf{R}}^\dagger \hat{a}_{\mathbf{R}}$ are, respectively, the annihilation and number operators in the lattice site \mathbf{R} . The amplitudes are, respectively, the two-body interaction strength, $h(\mathbf{R}) = U/2$, and the tunnel amplitude $J(\mathbf{R}, \mathbf{R}') = J$. For spin models, the operators \hat{K}_j represent spin operators, namely $\hat{K}_1(\mathbf{R}) \equiv \hat{S}_{\mathbf{R}}^z$ and $\hat{K}_2(\mathbf{R}, \mathbf{R}') \equiv \hat{S}_{\mathbf{R}}^x \cdot \hat{S}_{\mathbf{R}'}^x$ (Ising model) or $\hat{K}_2(\mathbf{R}, \mathbf{R}') \equiv \hat{S}_{\mathbf{R}}^x \cdot \hat{S}_{\mathbf{R}'}^x + \hat{S}_{\mathbf{R}}^y \cdot \hat{S}_{\mathbf{R}'}^y$ (XY model). Then $h(\mathbf{R})$ is the magnetic field and $J(\mathbf{R}, \mathbf{R}')$ the spin-exchange amplitude.

The dynamics is induced by a quench protocol (see for instance Refs. [4, 5, 33, 35]): After preparing the system in the ground state of some initial (pre-quench) Hamiltonian \hat{H}_0 , the Hamiltonian is abruptly changed to the final (post-quench) value \hat{H} at time $t = 0$. The latter governs the resulting unitary evolution of the system. It may be studied by measuring either response functions, $C(\mathbf{R}, t) = -i\langle [\hat{A}_X(t), \hat{B}_Y(0)] \rangle$, or equal-time correlation functions, $G(\mathbf{R}, t) \equiv \langle \hat{A}_X(t) \hat{B}_Y(t) \rangle - \langle \hat{A}_X(t) \rangle \langle \hat{B}_Y(t) \rangle$, where \hat{A}_X and \hat{B}_Y are two local operators acting on the finite sublattices X and Y separated by the distance \mathbf{R} . Here, we focus on particle or spin correlation functions, which are accessible in present-day experiments [4, 5, 33, 35]. Our results are, however, straightforwardly extended to response functions.

The starting point of our analysis is the observation that the system's dynamics is driven by the many-body excitations of the post-quench Hamiltonian. In the most-relevant low-energy sector of the spectrum, they may be assumed to be quasi-particle excitations. Assuming discrete-space translation invariance within the lattice, they are plane waves with well-defined quasi-momentum \mathbf{k} and energy $E_{\mathbf{k}}$. The correlation function may thus be

generically written

$$G(\mathbf{R}, t) = g(\mathbf{R}) - \int_{\mathcal{B}} \frac{d\mathbf{k}}{(2\pi)^D} \mathcal{F}(\mathbf{k}) \frac{e^{i(\mathbf{k} \cdot \mathbf{R} + 2E_{\mathbf{k}}t)} + e^{i(\mathbf{k} \cdot \mathbf{R} - 2E_{\mathbf{k}}t)}}{2} \quad (2)$$

where we set \hbar to unity and the integral spans the first Brillouin zone \mathcal{B} owing to lattice periodicity. In the remainder of this work, we disregard the quantity $g(\mathbf{R})$ since it does not contribute to the time evolution and we assume isotropic couplings. Equation (2) represents the motion of counter-propagating quasi-particle pairs, with velocities determined by the after-quench dispersion relation $E_{\mathbf{k}}$, and an amplitude $\mathcal{F}(\mathbf{k})$ that is constructed from the overlap of the initial state, the quasi-particle amplitudes, and the operators \hat{A}_X and \hat{B}_Y . Formally, Eq. (2) can be derived explicitly in exactly-solvable models. An important example is that of quadratic theories, which can be diagonalized by means of Bogoliubov transformations. Many models can be mapped into this form, using canonical transformations, meanfield approaches or spin-wave theories (see for instance Refs. [7, 37, 39–43] for examples in the context of out-of-equilibrium dynamics). For non exactly-solvable models, one may resort on numerical calculations, e.g. exact diagonalization or tensor-network techniques [44, 45].

Short-range couplings. – To start with, it is instructive to consider the case where the quasi-particle group velocity is bounded. It applies to models with couplings restricted to the nearest-neighbor lattice sites or decaying sufficiently fast (e.g. exponentially or algebraically with a large-enough exponent α [37–40]). The integral in Eq. (2) is evaluated using the stationary-phase approximation. In the infinite time and distance limit along the line $R/t = \text{const}$, it is dominated by the momentum contributions with a stationary phase (sp), *i.e.* $\nabla_{\mathbf{k}}(kR \mp 2E_{\mathbf{k}}t) = 0$ or, equivalently,

$$2V_{\mathbf{g}}(k_{\text{sp}}) = \pm R/t, \quad (3)$$

where $V_{\mathbf{g}} = \nabla_{\mathbf{k}} E_{\mathbf{k}}$ is the group velocity. Since the latter is bounded in the (finite) Brillouin zone, it has a maximum $V_{\mathbf{g}}^*$ and Eq. (3) may have a solution k_{sp} or not. For $R/t < 2V_{\mathbf{g}}^*$, Eq. (3) admits a solution and the correlation function reads [46]

$$G(R, t) \propto \frac{\mathcal{F}(k_{\text{sp}})}{(|\nabla_{\mathbf{k}}^2 E_{k_{\text{sp}}}| t)^{\frac{D}{2}}} \cos\left(k_{\text{sp}} R - 2E_{k_{\text{sp}}} t + \frac{\pi}{4}\right). \quad (4)$$

For $R/t > 2V_{\mathbf{g}}^*$, $G(R, t)$ is vanishingly small. The correlations are thus activated ballistically at the time $t = R/2V_{\mathbf{g}}^*$, which defines a linear LR edge characterized by the velocity $V_{\text{LR}} = 2V_{\mathbf{g}}^*$. This result is consistent with the Calabrese-Cardy picture [2]. Note that for $k^* \neq 0$, the quantity $\mathcal{F}(k^*)$ is in general finite while $|\nabla_{\mathbf{k}}^2 E_{k^*}|$ vanishes. Hence the amplitude of $G(R, t)$ diverges on the cone, which indicates a sharp LR edge.

Yet, Eq. (4) does not characterize only the LR edge but also a series of local maxima corresponding to those of the cosine function. In the vicinity of the LR cone, only the quasi-particles moving at the maximum group velocity contribute, which selects the momenta $k \simeq k^*$. There the maxima (m), defined by the equation $k^*R - 2E_k^*t = \text{const}$, propagate at the velocity $V_m = 2V_\varphi^* \equiv 2E_{k^*}^*/k^*$, *i.e.* twice the phase velocity at the maximum of the group velocity, k^* . Since the phase and group velocities are generally different, the LR cone is expected to feature a double structure characterized by these two velocities.

To illustrate it, consider the Bose-Hubbard model. In the superfluid regime, we may use a mean-field approximation. It yields a correlation function of the form (2) and the dispersion relation $E_k \simeq 2\sqrt{2J \sin^2(k/2) [2J \sin^2(k/2) + nU]}$ where n is the average number of bosons per site [39, 42]. This dispersion relation is bounded and the group velocity has a local maximum at some momentum $0 < k^* < \pi$, see inset of Fig. 1(a). Figure 1(a) shows the correlation function versus distance and time for $Un = 0.5J$. It shows a clear locality cone, determined by the LR velocity $V_{\text{LR}} \simeq 2V_g^*$ (solid green line). Moreover, the correlation map displays a series of parallel local maxima propagating at approximately twice the phase velocity at the momentum k^* , $V_m \simeq 2V_\varphi^*$ (dashed blue lines). These results are confirmed in Fig. 1(c) where we compare the values of the velocities found from fits to the correlation edge (V_{LR}) and local maxima (V_m) on the one hand, to twice the group (V_g^*) and phase (V_φ^*) velocities at k^* on the other hand. This result allows us to interpret previously unexplained results. Hence, the propagation velocities extracted from t-VMC calculations in Ref. [8] are in quantitative agreement with the value $2V_\varphi^*$ found here, and should thus be assimilated to the propagation of local maxima, *i.e.* to the inner structure of the causal region [47]. In contrast, the true LR edge is determined by the raise of the envelop of these maxima at the velocity $2V_g^*$ ($> 2V_\varphi^*$). An inner structure of local maxima moving with a velocity slower than twice the maximum group velocity is also observable in numerical t-DMRG results for a quench in the superfluid regime of the Fermi-Hubbard model [6], which may be explained similarly.

Experimental observation of the LR cone has been reported for a quench to the Mott-insulator regime [4]. The quench was performed close to the critical point where there exists a single characteristic velocity and no inner structure was observed. A richer behavior occurs deeper in the Mott regime, where the pair dispersion relation is strongly gapped, $2E_k^* \simeq U - 2(2n+1)J \cos(k)$ [48], see inset of Fig. 1(b). The maximum of the group velocity is at the center of the band, $k_{\text{max}}^* = \pi/2$, where $V_g^* = (2n+1)J$ and $V_\varphi^* = U/\pi$. Hence, for $U > \pi(2n+1)J$, the phase velocity exceeds the group velocity at k^* . As shown in Fig. 1(b), we then find a double structure where the local

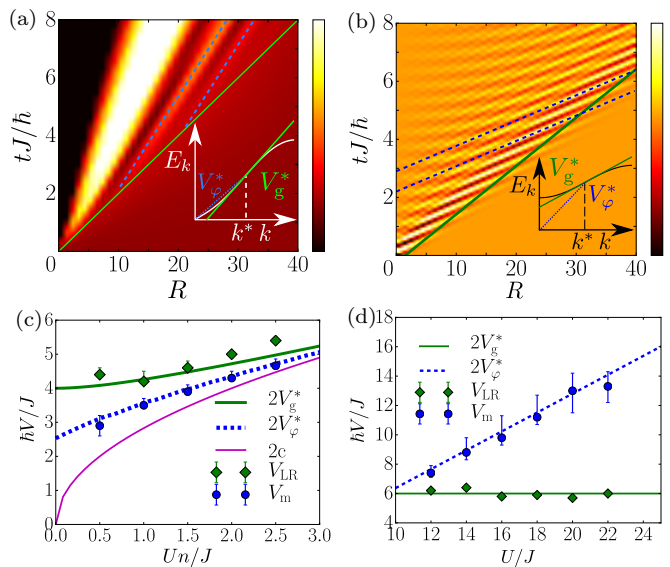


Figure 1. Upper panel: Spreading of the connected one-body correlation function $G(R, t) = \langle \hat{a}_R^\dagger(t) \hat{a}_0(t) \rangle - \langle \hat{a}_R^\dagger(0) \hat{a}_0(0) \rangle$ calculated from Eq. (2) for the one-dimensional Bose-Hubbard model. (a) Superfluid phase for a quench from the initial value $U_i n = J$ to the final value $U_f n = 0.5J$. (b) Mott-insulator phase with $n = 1$ for a quench from $U_i = \infty$ to $U_f = 18J$. In both cases, the spreading shows a linear causal LR cone, whose velocity is twice the maximum group velocity, $V_{\text{LR}} \simeq 2V_g^*$ (solid green line), and a series of parallel maxima propagating at twice the corresponding phase velocity, $V_m = 2V_\varphi^*$ (dashed blue lines). Lower panel: Comparison between the maximum group velocity (V_g^* , solid green line), the corresponding phase velocity (V_φ^* , dashed blue line), the sound velocity (c , dotted purple line) for reference, and fits to the LR cone velocity (V_{LR} , green diamonds) and the velocity of the maxima (V_m , blue disks) for the (c) superfluid and (d) Mott insulator phases with the same initial values as for (a) and (b).

maxima propagate faster than the LR cone, and vanish when reaching it. Again, we find that the local maxima are governed by the phase velocity, $V_m \simeq 2V_\varphi^*$, and the LR edge by the group velocity, $V_{\text{LR}} \simeq 2V_g^*$, see Fig. 1(d).

Long-range couplings. – We now turn to systems with long-range interactions. Power-law couplings $J_{\mathbf{R}, \mathbf{R}'} \sim J/|\mathbf{R} - \mathbf{R}'|^\alpha$ with a sufficiently small exponent α may produce several types of spectral divergences. Here, we assume that the spectrum is regular in the whole Brillouin zone, except in one point, which, up to appropriate gauge transformation, can be located in the infrared limit, $k = 0$. There, the dispersion relation may be written $E_k \simeq \Delta + ck^z$, with z the dynamical exponent and Δ the (possibly vanishing) gap. We focus on the case where the quasi-particle energy E_k is bounded but the group velocity $V_g(k)$ diverges, *i.e.* $0 < z < 1$. This case applies to various models where locality and its breaking has been discussed [33–41, 43, 49], for instance to spin models where Eq. (2) can be explicitly written within

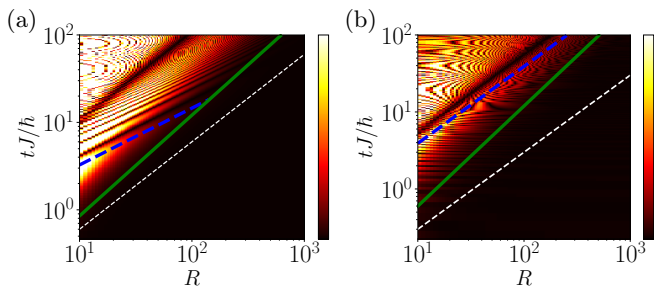


Figure 2. Spreading of the connected spin correlation function $G(R, t) = G_0(R, t) - G_0(R, 0)$ calculated from Eq. (2) for the following one-dimensional models: (a) LRXY model, $G_0(R, t) = \langle S_R^z(t) S_0^z(t) \rangle - \langle S_R^z(t) \rangle \langle S_0^z(t) \rangle$ for a quench from the ground state of the XXZ model, and (b) LRTI model, $G_0(R, t) = \langle S_R^x(t) S_0^x(t) \rangle - \langle S_R^x(t) \rangle \langle S_0^x(t) \rangle$ for the quench from $J_i/h = 0.25$ to $J_f/h = 0.5$. They feature a double algebraic structure (straight lines log-log scale). For both models, the LR edge is sub-ballistic, $t^* \propto R^{\beta_{\text{LR}}}$ with $\beta_{\text{LR}} > 1$, see solid green line. The thin white dashed line shows ballistic spreading for reference. For the (gapless) LRXY model, the inner structure shows super-ballistic propagation of the local maxima, $t_m \propto R^{\beta_m}$ with $\beta_m < 1$, see dashed blue line in panel (a). For the (gapped) LRTI model, the local maxima propagate ballistically, $t_m \propto R^{\beta_m}$ with $\beta_m = 1$, see dashed blue line in panel (b).

linear spin wave theory (LSWT).

Figure 2 shows the correlation function for two different spins models. The left panel corresponds to the LRXY model. Owing to continuous spin rotation symmetry, it is gapless, $\Delta = 0$, and $z = (\alpha - D)/2$ for $D < \alpha < D + 2$ [50]. The right panel corresponds to the LRTI model, where the transverse magnetic field opens a gap, $\Delta > 0$, and $z = \alpha - D$ for $D < \alpha < D + 1$ [37, 39, 40]. For both models, we find a double structure reminiscent of that discussed above for short-range models, although with important differences. First, the LR edge is not linear but algebraic (note the log-log scales in Fig. 2). While the known extended LR bounds [31, 32] are all super-ballistic, we find a clear *sub-ballistic* LR edge, $t \sim R^{\beta_{\text{LR}}}$ with $\beta_{\text{LR}} > 1$. Second, the inner structure shows a strongly model-dependent behavior: For the LRXY model, the correlation maxima are *super-ballistic*, $t \sim R^{\beta_m}$ with $\beta_m < 1$. For the LRTI, they are *ballistic*, $t \sim R$.

To understand these behaviors, let us proceed as before. Using stationary-phase approximation, we find Eq. (4) and the leading contribution along the line with a fixed ratio R/t is again given by Eq. (3). In the present case, however, the group velocity, $V_g(k) = cz/k^{1-z}$ diverges in the infrared limit. Hence, for any combination of t and R there is a quasi-particle with the corresponding group velocity, determined by the momentum $k_{\text{sp}} = (2czt/R)^{1/(1-z)}$. The LR edge is thus dominated by the infrared divergence, and, in contrast to the short-range case, we have to take into account the behavior of

the function \mathcal{F} in that limit. Assuming the power law scaling $\mathcal{F}(k) \sim k^\nu$ and inserting the above expressions into Eqs. (3) and (4), we then find

$$G_c(\mathbf{R}, t) \propto \frac{t^\gamma}{R^\chi} \cos \left[A_z \left(\frac{t}{R^z} \right)^{\frac{1}{1-z}} - 2\Delta t + \frac{\pi}{4} \right], \quad (5)$$

with $\gamma = \frac{\nu+D/2}{1-z}$, $\chi = \frac{\nu+D(2-z)/2}{1-z}$, and $A_z = 2c(1-z)(2cz)^{\frac{1}{1-z}}$. We can then deduce the double structure.

On the one hand, the LR edge is found by imposing that the amplitude of the correlation function becomes of the order of unity. It yields the algebraic form

$$t^* \propto R^{\beta_{\text{LR}}}, \quad \beta_{\text{LR}} = \chi/\gamma. \quad (6)$$

It immediately follows that, in general, the scaling of the LR edge does not depend only on the dispersion relation via the dynamical exponent z but also on the considered correlation function via the exponent ν , and on the dimension D . This contrasts with the short-range case, where a ballistic propagation independent of the dimension and of the observable is found [51]. Note also that $\chi = \gamma + D/2$. Hence, if the function $\mathcal{F}(k)$ does not diverge too fast, *i.e.* $\nu > -D/2$, the LR edge is always sub-ballistic. For the LRXY model and spin-spin correlations, we have $\nu = z = (\alpha - D)/2$, which yields $\beta_{\text{LR}} = 1 + \frac{D}{2\alpha}(2 + D - \alpha)$. For $\alpha = 2.3$ and $D = 1$, we find $\beta_{\text{LR}} \simeq 1.15$, in excellent agreement with the numerical calculations, see solid green line in Fig. 2(a) [52].

For the LRTI model, we have $z = \alpha - D$ and $\nu = 0$. It yields the sub-ballistic exponent $\beta_{\text{LR}} = 2 - z = 2 + D - \alpha$. It is completely determined by the dynamical exponent z and independent of the dimension D . For $\alpha = 1.7$ and $D = 1$, we find $\beta_{\text{LR}} = 1.3$, in good agreement with the numerical calculations, see solid green line in Fig. 2(b). Note that the above prediction matches the exact result of Ref. [39] for $D = 1$ and $\alpha = 3/2$ (*i.e.* $z = 1/2$), also confirmed by t-VMC calculations, and it is in fair agreement with the analysis of Ref. [40] for the 1D and 2D LRTI models.

On the other hand, the inner structure of the causal region is determined by the local maxima of the cosine function in Eq. (5). In contrast to the LR edge, it does not depend on the observable, *i.e.* on the amplitude function $\mathcal{F}(k)$. In contrast, it depends explicitly on whether the dispersion relation is gapped or not. For a gapless system ($\Delta = 0$), we find

$$t_m \propto R^{\beta_m}, \quad \beta_m = z. \quad (7)$$

We thus find that the correlation maxima are always super-ballistic. For the LRXY model and $\alpha = 2.3$, Fig. 2(a), we find the theoretical value $\beta_m = 0.65$. In the numerics, we study the internal structure of the correlation function by tracking the position of the first local maximum. For every value of the distance R we

determine the time at which the first maximum appears $\tau_m(R)$. We then fit the function with the ansatz $\tau_m = a * R^{\beta_{\text{fit}}} + b$ and extract the value of the exponent β_{fit} . For the parameters of Fig. 2(a), we find $\beta_{\text{fit}} \simeq 0.642 \pm 0.013$, in excellent agreement with the theoretical value, see dashed blue line. It is also in qualitative agreement the experimental observation of super-ballistic dynamics in the 1D LRXY model realized with trapped ion chains [33] and in rough agreement with the analysis of numerical calculations performed within the truncated Wigner approximation for 1D and 2D LRXY models [34]. The same result as Eq. (7) was found in Ref. [43], which appeared while completing the present work. Our analysis shows that this super-ballistic behavior characterizes the inner structure but not the LR edge as discussed above.

For a gapped system ($\Delta > 0$), the momentum dependence of the dispersion relation becomes irrelevant in the infrared limit. Hence the argument of the cosine function in Eq. (5) is constant in the large t limit for $t \propto R$. It follows that the local maxima are here always ballistic. This case applies to the LRTI model and the results of our numerical analysis are in excellent agreement with this prediction, see Fig. 2(b) where a fit to the first local maximum yields $\beta_{\text{fit}} \simeq 1.01 \pm 0.05$, see dashed blue line. This result explains the ballistic dynamics observed in the 1D LRTI model realized with trapped ion chains [35].

Conclusion and outlook. – The double structure of the causal region has fundamental consequences on the propagation of information in quantum systems with variable range interactions. Observation of both the outer and inner structures gives useful insight on microscopic properties. For short-range interactions, they are directly related to the group and phase velocities of the relevant many-body quasi-particles. For long-range interactions, their universal scaling laws are related to various spectral properties. The LR edge defines the causal region. For a bounded spectrum, it is observable dependent and always sub-ballistic, owing to destructive interference of quasi-particle contributions with arbitrary large group velocities, except for observables with a very strong infrared divergence. In turn local maxima that propagate ballistically close to the LR edge signal a gapped spectrum while a gapless spectrum induces super-ballistic propagation.

From an experimental or numerical point of view, observation of the LR edge requires careful analysis of the long-time and long-distance decay of the signal. It may be performed using the so-called ϵ -method as used in Refs [40, 41]. It consists in imposing a threshold ϵ on the signal, determine the activation time $t_\epsilon^*(R)$ as a function of distance R at this threshold, and evaluate it in the limit $\epsilon \rightarrow 0^+$, down to a few percent. In practice, however, it is easier to observe the dynamics of local maxima, as done usually. Our predictions for local maxima are consistent with several previous numeri-

cal and experimental observations. Since the local maxima are faster (ballistic or super-ballistic) than the LR edge (sub-ballistic), the latter may be observed by analyzing the space or time decay of the local maxima. It can be found using the amplitude of the correlation function in Eq. (5) and the scaling of dynamics of the local maxima. For a gapless system, we have $t_m \sim R^z$, and we find $\max\{G_c(R, t)\} \sim 1/t^{(\nu+D)/z} \sim 1/R^{\nu+D}$. For a gapped system, we have $t_m \sim R$, and we find $\max\{G_c(R, t)\} \sim 1/t^{D/2} \sim 1/R^{D/2}$.

We thank Anton Buyskikh and Jad C. Halimeh for stimulating discussions. This research was supported by the European Commission FET-Proactive QUIC (H2020 grant No. 641122) and Deutsche Forschungsgemeinschaft (DFG) through SFB/CRC1073 (Projects B03 and C03). It was performed using HPC resources from GENCI-CCRT/CINES (Grant c2015056853).

-
- [1] E. H. Lieb and D. W. Robinson, *Comm. Math. Phys.* **28**, 251 (1972).
 - [2] P. Calabrese and J. Cardy, *Phys. Rev. Lett.* **96**, 136801 (2006).
 - [3] S. Bravyi, M. B. Hastings, and F. Verstraete, *Phys. Rev. Lett.* **97**, 050401 (2006).
 - [4] M. Cheneau, P. Barmettler, D. Poletti, M. Endres, P. Schauss, T. Fukuhara, C. Gross, I. Bloch, C. Kollath, and S. Kuhr, *Nature (London)* **481**, 484 (2012).
 - [5] T. Fukuhara, P. Schausz, M. Endres, S. Hild, M. Cheneau, I. Bloch, and C. Gross, *Nature (London)* **502**, 76 (2013).
 - [6] S. R. Manmana, S. Wessel, R. M. Noack, and A. Muramatsu, *Phys. Rev. B* **79**, 155104 (2009).
 - [7] P. Barmettler, D. Poletti, M. Cheneau, and C. Kollath, *Phys. Rev. A* **85**, 053625 (2012).
 - [8] G. Carleo, F. Becca, L. Sanchez-Palencia, S. Sorella, and M. Fabrizio, *Phys. Rev. A* **89**, 031602(R) (2014).
 - [9] V. Bendkowsky, B. Butscher, J. Nipper, J. P. Shaffer, R. Läuchli, and T. Pfau, *Nature (London)* **458**, 1005 (2009).
 - [10] H. Weimer, M. Müller, I. Lesanovsky, P. Zoller, and H. P. Büchler, *Nat. Phys.* **6**, 382 (2010).
 - [11] P. Schausz, M. Cheneau, M. Endres, T. Fukuhara, S. Hild, A. Omran, T. Pohl, C. Gross, S. Kuhr, and I. Bloch, *Nature (London)* **491**, 87 (2012).
 - [12] A. Browaeys, D. Barredo, and T. Lahaye, *J. Phys. B: At. Mol. Opt. Phys.* **49**, 152001 (2016).
 - [13] O. Firstenberg, T. Peyronel, Q.-Y. Liang, A. V. Gorshkov, M. D. Lukin, and V. Vuletic, *Nat. Phys.* **502**, 71 (2013).
 - [14] A. Micheli, G. K. Brennen, and P. Zoller, *Nat. Phys.* **2**, 341 (2006).
 - [15] B. Yan, S. A. Moses, B. Gadway, J. P. Covey, K. R. A. Hazzard, A. M. Rey, D. S. Jin, and J. Ye, *Nature (London)* **501**, 521 (2013).
 - [16] S. A. Moses, J. P. Covey, M. T. Miecnikowski, D. S. Jin, and J. Ye, *Nat. Phys.* **13**, 13 (2017).
 - [17] A. Griesmaier, J. Werner, S. Hensler, J. Stuhler, and T. Pfau, *Phys. Rev. Lett.* **94**, 160401 (2005).

- [18] Q. Beaufils, R. Chicireanu, T. Zanon, B. Laburthe-Tolra, E. Maréchal, L. Vernac, J.-C. Keller, and O. Gorceix, *Phys. Rev. A* **77**, 061601 (2008).
- [19] M. Lu, N. Q. Burdick, S. H. Youn, and B. L. Lev, *Phys. Rev. Lett.* **107**, 190401 (2011).
- [20] S. Baier, M. J. Mark, D. Petter, K. Aikawa, L. Chomaz, Z. Cai, M. Baranov, P. Zoller, and F. Ferlaino, *Science* **352**, 201 (2016).
- [21] T. Lahaye, C. Menotti, L. Santos, M. Lewenstein, and T. Pfau, *Rep. Prog. Phys.* **72**, 126401 (2009).
- [22] A. A. Houck, H. E. Tureci, and J. Koch, *Nat. Phys.* **8**, 292 (2012).
- [23] X.-L. Deng, D. Porras, and J. I. Cirac, *Phys. Rev. A* **72**, 063407 (2005).
- [24] R. Islam, E. Edwards, K. Kim, S. Korenblit, C. Noh, H. Carmichael, G.-D. Lin, L.-M. Duan, C.-C. Joseph Wang, J. Freericks, and C. Monroe, *Nat. Comm.* **2**, 377 (2011).
- [25] B. P. Lanyon, C. Hempel, D. Nigg, M. Müller, R. Gerritsma, F. Zähringer, P. Schindler, J. T. Barreiro, M. Rambach, G. Kirchmair, M. Hennrich, P. Zoller, R. Blatt, and C. F. Roos, *Science* **334**, 57 (2011).
- [26] C. Schneider, D. Porras, and T. Schaetz, *Rep. Prog. Phys.* **75**, 024401 (2012).
- [27] R. Blatt and C. F. Roos, *Nat. Phys.* **8**, 277 (2012).
- [28] L. Childress, M. V. Gurudev Dutt, J. M. Taylor, A. S. Zibrov, F. Jelezko, J. Wrachtrup, P. R. Hemmer, and M. D. Lukin, *Science* **314**, 281 (2006).
- [29] G. Balasubramanian, P. Neumann, D. Twitchen, M. Markham, R. Kolesov, N. Mizuochi, J. Isoya, J. Achard, J. Beck, J. Tessler, V. Jacques, P. R. Hemmer, F. Jelezko, and J. Wrachtrup, *Nat. Mater.* **8**, 383 (2009).
- [30] F. Dolde, I. Jakobi, B. Naydenov, N. Zhao, S. Pezzagna, C. Trautmann, J. Meijer, P. Neumann, F. Jelezko, and J. Wrachtrup, *Nat. Phys.* **9**, 139 (2013).
- [31] M. B. Hastings and T. Koma, *Comm. Math. Phys.* **265**, 781 (2006).
- [32] M. Foss-Feig, Z.-X. Gong, C. W. Clark, and A. V. Gorshkov, *Phys. Rev. Lett.* **114**, 157201 (2015).
- [33] P. Richerme, Z.-X. Gong, A. Lee, C. Senko, J. Smith, M. Foss-Feig, S. Michalakis, A. V. Gorshkov, and C. Monroe, *Nature (London)* **511**, 198 (2014).
- [34] J. Schachenmayer, A. Pikovski, and A. M. Rey, *New J. Phys.* **17**, 065009 (2015).
- [35] P. Jurcevic, B. P. Lanyon, P. Hauke, C. Hempel, P. Zoller, R. Blatt, and C. F. Roos, *Nature (London)* **511**, 202 (2014).
- [36] J. Schachenmayer, B. P. Lanyon, C. F. Roos, and A. J. Daley, *Phys. Rev. X* **3**, 031015 (2013).
- [37] P. Hauke and L. Tagliacozzo, *Phys. Rev. Lett.* **111**, 207202 (2013).
- [38] J. Eisert, M. van den Worm, S. R. Manmana, and M. Kastner, *Phys. Rev. Lett.* **111**, 260401 (2013).
- [39] L. Cevolani, G. Carleo, and L. Sanchez-Palencia, *Phys. Rev. A* **92**, 041603(R) (2015).
- [40] L. Cevolani, G. Carleo, and L. Sanchez-Palencia, *New J. Phys.* **18**, 093002 (2016).
- [41] A. S. Buyskikh, M. Fagotti, J. Schachenmayer, F. Essler, and A. J. Daley, *Phys. Rev. A* **93**, 053620 (2016).
- [42] S. S. Natu and E. J. Mueller, *Phys. Rev. A* **87**, 053607 (2013).
- [43] I. Frérot, P. Naldesi, and T. Roscilde, “Multi-speed prethermalization in spin models with power-law decaying interactions,” (2017), arXiv:1704.04461.
- [44] J. Haegeman, B. Pirvu, D. J. Weir, J. I. Cirac, T. J. Osborne, H. Verschelde, and F. Verstraete, *Phys. Rev. B* **85**, 100408 (2012).
- [45] N. Nakatani, S. Wouters, D. V. Neck, and G. K.-L. Chan, *J. Chem. Phys.* **140**, 024108 (2014).
- [46] For simplicity, we assume that, if it exists, there is a single solution \mathbf{k}_{sp} . Should Eq. (3) have several solutions, Eq. (4) is replaced by the sum of the corresponding contributions.
- [47] Note that no clear double structure is visible on Fig. 1(a) of Ref. [8] because it corresponds to $Un = 4$ where the group and phase velocities are almost equal.
- [48] S. D. Huber, E. Altman, H. P. Büchler, and G. Blatter, *Phys. Rev. B* **75**, 085106 (2007).
- [49] M. Gessner, V. M. Bastidas, T. Brandes, and A. Buchleitner, *Phys. Rev. B* **93**, 155153 (2016).
- [50] I. Frérot, P. Naldesi, and T. Roscilde, “Entanglement and fluctuations in the XXZ model with power-law interactions,” (2017), arXiv:1703.01799.
- [51] Note that the dependence on D and ν completely disappears in the limit of a spectrum with a non-divergent velocity, $z \rightarrow 1^-$, in agreement with the general LR picture [1].
- [52] In the numerics, the LR edge is determined imposing a threshold of 1% (LRXY) or 3% (LRTI) on the correlation function and then fitting it with an algebraic ansatz with the exponent fixed to the theoretical value $\beta_{\text{LR}} = \chi/\gamma$. The lines are then plotted in log-log scale in Figs. 2(a) and (b), showing excellent agreement with the observed LR edge.